Taylor & Francis
Taylor & Francis Group

Check for updates

Reduced-order modelling of thermoacoustic instabilities in a two-heater Rijke tube

Chandrachur Bhattacharya[a], Sudeepta Mondal[a,b], Asok Ray[a,b*] and
Achintya Mukhopadhyay[c]

[a]*Department of Mechanical Engineering, The Pennsylvania State University, University Park, PA,
USA;* [b]*Department of Mathematics, The Pennsylvania State University, University Park, PA, USA;*
[c]*Department of Mechanical Engineering, Jadavpur University, Kolkata, India*

The topic of thermoacoustic instabilities in combustors is well-investigated, as it is
important in the field of combustion, primarily in gas-turbine engines. In recent years,
much attention has been focused on monitoring, diagnosis, prognosis, and control of
high-amplitude pressure oscillations in confined combustion chambers. The Rijke tube
is one of the most simple, yet very commonly used, laboratory apparatuses for emula-
tion of thermoacoustic instabilities, which is also capable of capturing the physics of
the thermally driven acoustics. A Rijke tube apparatus can be constructed with an elec-
trical heater acting as the heat source, thus making it more flexible to operate and safer
to handle than a fuel-burning Rijke tube or a fuel-fired combustor. Augmentation of the
heat source of the Rijke tube with a secondary heater at a downstream location facili-
tates better control of thermoacoustic instabilities. Along this line, much work has been
reported on the investigation of thermoacoustics by using computational fluid dynamics
(CFD) modelling as well as reduced-order modelling for both single-heater and two-
heater Rijke tube systems. However, since reduced-order models are often designed and
built upon certain empirical relations, they may not account for the dynamic behaviour
of the heater itself, which is a critical factor in the analysis and synthesis of real-time
robust control systems. This issue is addressed in the current paper, where modifica-
tions have been made to existing models by incorporating heater dynamics. The model
results are systematically validated with experimental data, generated from an in-house
(electrically heated) Rijke tube apparatus.

Keywords: thermoacoustic instability; Rijke tube apparatus; reduced-order modelling

1. Introduction

The prime source of thermoacoustic instabilities (TAI) [1] in a combustor is the strong
coupling between the unsteady heat release rate from fuel-air burning and natural acous-
tics in the confined combustion chamber. The TAI phenomena lead to high-amplitude
pressure oscillations (e.g. peak values reaching ~ 1000 Pa) in the combustion chamber,
which could be detrimental to the structural integrity of the combustor as these oscillations
may produce thermomechanical fatigue stresses in the combustor wall and liners. The TAI
phenomena also cause disruptions in the air flow through the combustor, often leading to
flow reversal (which affects both upstream and downstream components in the combustion

*Corresponding author. Email: axr2@psu.edu

system as well) and instigating flame blowout. It is well known that a very small amount of energy from the combustion process may lead to TAI due to low acoustic damping in the combustors [2].

In recent years, much research has been conducted to investigate the nonlinear nature of acoustic waves within the combustion chamber. The Rijke tube [3] is one of the simplest experimental devices that can capture the essential physics of combustion chamber acoustics and their coupling with the heat release rate. A thorough experimental and numerical study on Rijke tubes has been conducted by [4]. Other researchers such as [5–7] have also conducted studies using a Rijke tube apparatus and have attempted to implement various control methods in order to reduce the severity of TAI. Several researches (e.g. [8–12]) have also conducted experimental research on TAI in fuel-burning laboratory-scale combustors. However, a major drawback of solely using an experimental apparatus for the purpose of extensive research is the lack of versatility and operating range, which is primarily due to safety requirements or limitations of the facilities at hand. Thus, there is a strong need for the development of reduced-order numerical models for the study of combustion instabilities in the framework of computational models of affordable complexity. [13] proposed a simplified reduced-order model based on the principle of Galerkin-type modal decomposition of the acoustic waves to solve the acoustic wave equation with a heat source. A similar method has been used by [14,15] for modelling the Rijke tube. Most current available Galerkin-based models try to account for the heater time lag using a variable τ (e.g. [16]). However this is a flow time lag and does not include the time response of the heater itself, i.e. the thermal inertia of the system or the dynamics of the heater; moreover, estimating of the parameter τ is not always easy. This may lead to moderately inaccurate response times, which is an important factor in designing a robust online active control system. In the research work reported in the current paper, the authors have attempted to modify the existing Galerkin-based numerical model to include heater and thermal dynamics as well as include some of the flow physics to provide more accurate time responses, while still retaining much lower model complexity than a full-scale computational fluid dynamics (CFD) simulation. In the models available in the literature, the user needs to specify parameters such as heater temperature, which cannot be directly controlled. The model, proposed in this paper, uses heater power as an input to the system, similar to the input that an experimental Rijke tube apparatus receives. Similarly, the reduced-order model is re-formulated such that, for the same model parameters, the entire range of operation of the Rijke tube can be simulated without re-tuning the critical parameters.

Several methods exist for suppression of the generated high-amplitude pressure oscillations in combustors. Passive control in the form of acoustic dampers [17] are widely used for mitigation of TAI. However, such acoustic dampers are only useful over certain frequency ranges, and they may not be effective at low frequencies. Several active control methods have also been proposed by researchers, such as the use of Helmholtz resonators [18], loudspeakers [7,14] and radial injection of air through micro-jets [19]. Usage of a secondary heat source has been introduced by [20] as a method of controlling the TAI based on the concept of destructive interference. This is a viable method of TAI control, especially for large combustors in aircraft and land-based gas turbines. Numerical simulations have been conducted in the current paper to investigate the efficacy of using a secondary (control) heater downstream for mitigating the instabilities of pressure oscillations in the Rijke tube.

Contributions: From the above perspectives, major contributions of the paper are summarised below.

(1) *Modification of established modal decomposition-based order reduction techniques*: The objective here is to include the effects of heater dynamics, system thermal inertia, and flow dynamics on the reduced-order model.
(2) *Modification of the simulation procedure for reduced-order modelling*: The objective here is to develop a numerically efficient procedure that takes into account the effects of time-varying thermal and flow conditions of the Rijke tube apparatus for numerical solution.
(3) *Demonstration of the efficacy of a secondary control heater as a method for suppressing the instabilities in the Rijke tube system*: The objective here is to show how the results of the numerical simulation compare to those reported in the standard literature.
(4) *Experimental validation of the proposed reduced-order modelling technique*: The objective here is to validate the aforesaid model against experimental results from an in-house Rijke tube and to show how the designed formulation works across the entire operational regime.

Organisation: The rest of the paper is organised into the following sections:

- Section 2 describes the Rijke tube apparatus that is used to produce the experimental data for validating the proposed numerical model.
- Section 3 presents the basic mathematical formulation of a reduced-order Galerkin-based model of the two-heater Rijke tube, where the modifications pertaining to the thermal inertia effects are also described. Section 3.4 validates the proposed numerical model with the results that are obtained from the experiments.
- Section 4 discusses the stability chart that is generated from the experimental data. Section 4.4 briefly discusses the hysteresis effects as seen in the numerical model, and also provides a comparison with the results of experimental studies that are reported in the literature.
- Section 5 demonstrates selected numerical simulations by using the secondary heater as a control mechanism for suppression of instabilities, where the results are compared to those available in the reported literature.
- Section 6 summarises and concludes the paper along with recommendations for future research.

2. The experimental Rijke tube apparatus

The experimental Rijke tube apparatus, which has been constructed in the laboratories of Penn State [21], consists of a 1.5 m long aluminium tube with a hollow square cross-section of inside lengths of 93 mm. There are two heating elements: a fixed primary heater at 0.375 m from the flow inlet and a movable secondary heater downstream. Both heaters are made of compact wire-mesh Nichrome for generating thermal power, which emulate the flame in a combustible fuel-air mixture in a real-life combustor. The secondary (control) heater has a maximum displacement of 500 mm from the centre of the tube towards the exit end. Figure 1 depicts the Rijke tube apparatus.

An array of eight wall-mounted pressure sensors are placed at equidistant axial locations for capturing the pressure signals. The Rijke tube data are acquired at a sampling rate
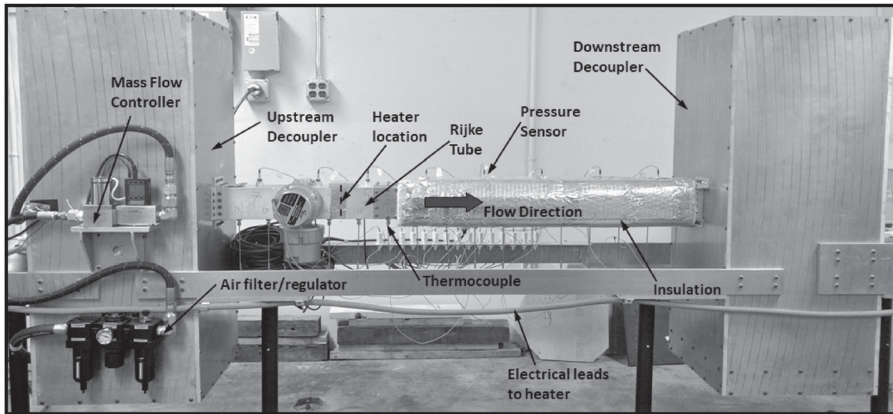
Figure 1.   Rijke tube experimental apparatus.

of 8192 Hz. To measure the spatio-temporal temperature variation, 15 K- type transition-junction thermocouple probes are used. The mass-flow rate into the system is controlled accurately using an Alicat Mass Flow Controller (0–1000 SLPM). The mass-flow rate controls not just the velocity over the heater but also affects the convective heat transfer from the wire mesh to the air and heat loss to the walls. The inlet and outlet of the tube are fitted with decouplers, which are large hollow enclosures serving the purpose of producing pressure waves under open-open end boundary conditions of the Rijke tube. Additionally, the upstream decoupler reduces flow fluctuations at the inlet while the downstream decoupler serves as a heat sink, allowing the hot air exiting the outlet to be cooled, before it is released to the atmosphere.

The two Nichrome heaters are capable of handling high heating loads for a sufficiently long time without being oxidised at the high operating temperatures. The square-weave 40-mesh structure of each heater acts as an acoustically compact source of thermal energy and allows a uniform heating of air over a cross-section. Two copper rods are welded to the copper strips and are electrically shielded from the walls of the chamber. The copper tubes are connected to a programmable DC power supply. The length of the tube downstream of the heater is insulated to prevent heat loss from the walls allowing for maintaining the same initial and running conditions of different experimental runs. It also acts as a safety measure to prevent the operator from coming in contact with the hot metal walls.

3.   Reduced-order numerical modelling of the Rijke tube

This section addresses reduced-order modelling of both single-heater and two-heater Rijke tubes, which include the thermal-hydraulic dynamics and their coupling with chamber acoustics.

3.1.   *Modelling of a single-heater Rijke tube*

As mentioned previously, a simplified reduced-order model using Galerkin-type modal decomposition was introduced by [13,22] to solve the acoustic wave equation with a heat source in the system. The one-dimensional wave equation was derived for the pressure

perturbations (p') as

$$\frac{\partial^2 p'}{\partial t^2} - a^2 \frac{\partial^2 p'}{\partial x^2} = (\gamma - 1) \frac{\partial \dot{Q}}{\partial t} \tag{1}$$

where a denotes the speed of sound and $\dot{Q}$ is the volumetric rate of thermal power addition. Equation (1) does not include the effects of mean flow on the acoustic field. Culick's expansion [13] is used for the pressure perturbations (p') and velocity perturbations (u') using the Galerkin eigen-acoustic modes. The decomposition into n modes having individual time-varying modal amplitudes of $\eta_j(t)$ yields:

$$p'(x, t) = \sum_{j=1}^{n} p'_j(x, t) = p_0 \sum_{j=1}^{n} \eta_j(t) \psi_j(x) \tag{2}$$

$$u'(x, t) = \sum_{j=1}^{n} u'_j(x, t) = \sum_{j=1}^{n} \frac{\dot{\eta}_j(t)}{\gamma k_j^2} \frac{\mathrm{d}\psi_j(x)}{\mathrm{d}x} \tag{3}$$

where p_0 is the mean undisturbed pressure; $\psi_j(x)$ and k_j are the mode shape (at the location x) and the wavenumber of the jth mode, respectively, which has a natural frequency of ω_j; and γ is the ratio of specific heats of air.

Substituting Equation (2) into Equation (1), expanding into eigen-modes, and adding a damping term ξ_j [23], the final expression is obtained as

$$\frac{\mathrm{d}^2 \eta_j}{\mathrm{d}t^2} + 2\xi_j \omega_j \frac{\mathrm{d}\eta_j}{\mathrm{d}t} + \omega_j^2 \eta_j = \frac{\gamma - 1}{p_0} \int \psi_j \frac{\partial \dot{Q}}{\partial t} \mathrm{d}x \tag{4}$$

where the left-hand expression in Equation (4) represents a set of n uncoupled linear oscillators that are excited by the forcing terms on the right-hand side. For a Rijke tube, [14] proposed a modified version of King's law, which yields the volumetric rate of heat addition ($\dot{Q}$) as

$$\dot{Q} = \frac{2L_w(T_w - \overline{T})}{SL\sqrt{3}} \sqrt{\pi \lambda C_v \rho_0 \frac{d_w}{2}} \left[\sqrt{\left| \frac{u_0}{3} + u'_f(t - \tau) \right|} - \sqrt{\left| \frac{u_0}{3} \right|} \right] \delta(x - x_f) \tag{5}$$

where L is the length of the Rijke tube, L_w is the equivalent length of the wire, λ is the thermal conductivity of air, C_v is the constant volume specific heat capacity of air, τ is the time lag between the heat transfer and the velocity as a result of thermal inertia, ρ_0 is the mean density of the Rijke tube air, d_w is the heater wire diameter, $(T_w - \overline{T})$ is the mean temperature difference between the heater and the air, S is the cross-sectional area of the Rijke tube, x_f is the heater location, and u'_f is the acoustic velocity perturbation at the heater location. Using Equation (5), the acoustic equation (Equation (4)) is modified to:

$$\frac{\mathrm{d}^2 \eta_j}{\mathrm{d}t^2} + 2\xi_j \omega_j \frac{\mathrm{d}\eta_j}{\mathrm{d}t} + \omega_j^2 \eta_j = \frac{\mathrm{d}\dot{Q}'}{\mathrm{d}t} \tag{6}$$

where $\dot{Q}'$ combines the remaining terms as

$$\dot{Q}' \triangleq \frac{2(\gamma - 1)L_w(T_w - \overline{T})}{p_0 SL\sqrt{3}} \sqrt{\pi \lambda C_v \rho_0 \frac{d_w}{2}} \left[\sqrt{\left| \frac{u_0}{3} + u'_f(t - \tau) \right|} - \sqrt{\left| \frac{u_0}{3} \right|} \right] \psi_j(x_f) \tag{7}$$

and the frequency-dependent damping ξ_j is given by [4] as

$$\xi_j \triangleq \left(c_1 \frac{\omega_j}{\omega_1} + c_2 \sqrt{\frac{\omega_1}{\omega_j}} \right) \tag{8}$$

where the first term in Equation (8) is responsible for the end losses and the second term represents losses due to boundary layers; and the constants c_1 and c_2 are the damping coefficients that represent the amount of acoustic damping in the Rijke tube. The time lag τ is computed by using Lighthill's correlation as: $\tau \simeq 0.2 \frac{d_w}{u_0}$.

The modal equations, derived above, can be cast in a linearised state-space form and the dimensionality of the ordinary differential equation (ODE) system depends on the number of the selected 'significant' acoustic modes. For each mode, there are two states, η_j and $\dot{\eta}_j$. This ODE system can be solved using a numerical method (e.g. Runge-Kutta).

3.2. *Modelling of a two-heater Rijke tube*

A secondary heat source is introduced in the Rijke tube in addition to the primary heat source, with the secondary heater acting as a control heater. This arrangement changes Equation (6) to now having two heat source terms:

$$\frac{d^2\eta_j}{dt^2} + 2\xi_j\omega_j\frac{d\eta_j}{dt} + \omega_j^2\eta_j = \frac{d\dot{Q}'_1}{dt} + \frac{d\dot{Q}'_2}{dt} \tag{9}$$

$$\dot{Q}'_i = \frac{2(\gamma - 1)L_w(T_{w,i} - \overline{T})}{p_0 SL\sqrt{3}} \sqrt{\pi \lambda C_v \rho_0 \frac{d_w}{2}}$$

$$\times \left[\sqrt{\left| \frac{u_0}{3} + u'_{f,i}(t - \tau_i) \right|} - \sqrt{\left| \frac{u_0}{3} \right|} \right] \psi_j(x_{f,i}), \quad i = 1, 2 \tag{10}$$

where the subscript i takes values 1 and 2 for the primary and secondary heaters, respectively.

3.3. *Modelling of the heater and thermal dynamics*

The state-space representation of the acoustics in Equation (4) for the jth mode is

$$\begin{bmatrix} \dot{\eta}_j \\ \ddot{\eta}_j \end{bmatrix} = \begin{bmatrix} 0 & 1 \\ -\omega_j^2 & -2\xi_j\omega_j \end{bmatrix} \begin{bmatrix} \eta_j \\ \dot{\eta}_j \end{bmatrix} + \begin{bmatrix} 0 \\ \frac{d\dot{Q}'_1}{dt} + \frac{d\dot{Q}'_2}{dt} \end{bmatrix} \tag{11}$$

where the frequency ω_j, computed from [13,24], is represented as

$$\omega_j = ak_j \tag{12}$$

where the wavenumber k_j is fixed for a given acoustic boundary condition with input–output specifications of a (pressure anti-node, or pressure open) fixed inlet velocity and (pressure node, or pressure closed) constant outlet pressure; and the speed of sound a is

a function of the gas temperature in the tube. In this case, the tube has constant pressures at either end, and the speed of sound a is approximated to depend on the mean gas temperature, which yields the following expressions for ω_j and ξ_j:

$$\omega_j = \sqrt{\gamma R\, T_{avg}} \left(j\frac{\pi}{L} \right) \tag{13}$$

$$\frac{\xi_j}{\xi_1} = \frac{\omega_j}{\omega_1} \tag{14}$$

Since ω_j directly depends on the time-dependent temperature T, the system matrix in Equation (11) is linear parameter varying (LPV) (which is effectively time varying) and hence needs to be recomputed at each time step.

For ease of computation, many researchers have used the above reduced-order equations by making certain approximations, such as the mean values of temperature and flow velocity, under the assumption that they are constants. However, this assumption may not always be appropriate, not only because of the temporal changes but also due to the rate of change of these time-dependent parameters. In the experimental apparatus, it may not be possible to control directly the temperature of the heaters, but instead the power input into the heater is the directly controllable variable and the temperature changes occur as a result of the power input and the heat transfer within the Rijke tube. Therefore, the temperature itself has its own dynamics, which has been addressed in this paper and included into the computational procedure.

In view of the above discussion, the heater power is the variable that is set by the user, and the temperatures evolve following the various relations of heat transfer and fluid mechanics. In the experimental apparatus, the power supply has its own transient behaviour, which is assumed to be linear within the operational range such that the heater is able to go from 0 to 2000 W in a linear ramp in 1 s; and this limits the rate of power rise or fall in the heaters. The rate of heat loss ($\dot{Q}_{heater}$) from the heater in a time step is computed from the following equation [15]:

$$\dot{Q}_{heater}(t) = L_w(T_{w,i} - \overline{T})\left[\lambda + 2\sqrt{\pi\lambda C_v \rho_0 \frac{d_w}{2}} \left(\left(1 - \frac{1}{3\sqrt{3}} \right)\sqrt{\overline{u}} \right.\right.$$
$$\left.\left. + \frac{1}{\sqrt{3}}\sqrt{\left| \frac{\overline{u}}{3} + u'(t-\tau) \right|} \right) \right] \tag{15}$$

So the temperature of the heater wire (T_w) changes in the time interval $[t,\ t+dt)$ as

$$T_w \leftarrow T_w + \frac{(P(t) - \dot{Q}_{heater}(t))\,dt}{MCp_{wire}(T_w)} \tag{16}$$

where M is the mass of the wire mesh that can be obtained by measurement; $P(t)$ is the time-dependant power supplied to the heater; and Cp_{wire} is the (temperature-dependent) specific heat capacity of the wire material, which is available from manufacturer's specifications. For computing the temperature in the Rijke tube, the flow domain in the tube is split into three segments; one containing the volume between the inlet and first heater, the next being the volume between the two heaters, and the third being the volume between the secondary heater and the outlet. It is assumed that the temperature in the first segment is always the same as the inlet temperature (T_{in}). The temperatures in the remaining

two sections are computed by doing energy flow analysis on the constant volume; $\dot{Q}_{add}$ is the power added to a segment in a time step, where the subscript *down* denotes the value downstream:

$$\dot{Q}_{add} = Cp(T_{down})T_{down}\dot{m}_{in} + \dot{Q}_{heater}(t) - \dot{Q}_{conv} - Cp(T_{segment})T_{segment}\dot{m}_{in} \qquad (17)$$

where $\dot{Q}_{conv}$ is the rate of heat loss to the Rijke tube wall of area $A_{segment}$ (which is at the inlet temperature) via convection.

$$\dot{Q}_{conv} = 0.664\lambda(Re_{segment})^{0.5}(Nu)^{0.333}A_{segment}(T_{segment} - T_{in}) \qquad (18)$$

Finally, the temperature of the volume segment $V_{segment}$ is computed in the time interval $[t, \ t + \mathrm{d}t)$ as

$$T_{segment} \leftarrow T_{segment} + \frac{\dot{Q}_{add}\,\mathrm{d}t}{\rho V_{segment}Cp(T_{segment})} \qquad (19)$$

The average temperature is measured as the segment length-weighted average of the segment temperatures.

Using all the above additional information that is computed by solving the heat transfer and certain fluid equations, the reduced-order model can be improved by removing some of the typical assumptions. Values of parameters (e.g. the mean temperature, wire temperature, density and velocity at the wire) now become functions of time and are dependent on the changing operating conditions of the Rijke tube. This is in agreement with what is observed experimentally as for the same heater input, the heater wire temperature is substantially higher when the flow rate is low due to lower convective heat transfer as opposed to higher flow rate situations. These physical processes also dictate mean temperature, speed of sound and the natural frequency of the system. Thus, a single model can be used for the entire operational range of the Rijke tube without having to make assumptions and change the individual variable values for each operating region. Furthermore, accounting for heater lag produces a more accurate time response of the system to changes in the control power and thus is better for studying transient phenomena or for testing the effectiveness of controllers on the system.

Equations (10) and (15) are modified to account for the local conditions of temperature and density as follows. The assumption here is that only the upstream values are considered when computing the heat transfer, where the subscripts *in* and *down* denote the values at the inlet and the downstream sections, respectively. It is noted that the model parameters C_v and λ are functions of temperature.

$$\dot{Q}_{heater}(t) = L_w(T_{w,i} - T_{down}) \times \left[\lambda + 2\sqrt{\pi\lambda(T)C_v(T)\rho_{in}\frac{T_{in}}{T_{down}}\frac{d_w}{2}}\right.$$

$$\left. \times \left(\left(1 - \frac{1}{3\sqrt{3}}\right)\frac{u_{in}T_{down}}{T_{in}} + \frac{1}{\sqrt{3}}\sqrt{\left|\frac{u_{in}T_{down}}{3T_{in}} + u'(t - \tau)\right|}\right)\right] \qquad (20)$$

$$\dot{Q}'_i = \frac{2(\gamma - 1)L_w(T_{w,i} - T_{down})}{\sqrt{3}p_{in}SL}\sqrt{\pi\lambda(T)C_v(T)\rho_{in}\frac{T_{in}}{T_{down}}\frac{d_w}{2}}$$

$$\times \left[\sqrt{\left|\frac{u_{in}T_{down}}{3T_{in}} + u'_{f,i}(t - \tau_i)\right|} - \sqrt{\left|\frac{u_{in}T_{down}}{3T_{in}}\right|}\right]\psi_j(x_{f,i}) \qquad (21)$$

The effects of uncertainties are realised in the simulation by modifying the acoustic velocity perturbation u' with a zero-mean additive Gaussian noise component that is chosen to have an intensity equal to 0.5% of the mean flow velocity.

3.4. *Parameterisation of the reduced-order model*

This section parameterises the reduced-order model, developed in Section 3, to match the Rijke tube apparatus described in Section 2. The geometry and other model parameters are chosen to be the same as those in the experimental apparatus. The length of the numerically modelled Rijke tube is taken to be $L = 1.5$ m, area of cross-section $S = 0.093 \times 0.093$ m^2. The primary heater is placed at $x_1 = 0.375$ m, similar to the experimental apparatus, and the pressure sensor is located at $x_p = 1$ m; all lengths are measured downstream from the inlet. The heaters have properties similar to the actual wire mesh used in the experiment with $L_w = 23.6$ m, $d_w = 0.33$ mm. The thermal heat capacity is taken to be that of Nichrome and each wire mesh has a total mass of $M = 170$ gm. The thermal properties of air used are fourth-order polynomials obtained from a NASA report (the NASA polynomials) [25].

In the numerical simulations reported in this paper, a total of 10 eigen-modes are considered to adequately capture the dynamics of the acoustic system. This implies that the number of eigen-modes is $n = 10$, as seen in Equations (2) and (3). To model the damping coefficients in Equation (8), the parameters c_1 and c_2 that are to be set by the user depend on the actual observed damping. These parameters have been set to be $c_1 = 0.048$ and $c_2 = 0.040$ to match the experimental results described in Section 4. Furthermore, the entire amount of the net heat transferred from the heater(s) enters the air, because a part of it is lost to the surroundings (primarily by radiation). Therefore, a factor $\alpha < 1$ is multiplied to the value of $Q(t)$. An empirical model of the parameter α is

$$\alpha = 1 - \left(\frac{T_w - T_{avg}}{T_w} \right)^{0.15} \tag{22}$$

The above formulation assumes the system to be acoustically closed. However, that is not actually true as though the presence of the decouplers maintain nearly constant pressures at the ends, the presence of a flow rate regulator ensures a constant flow. Thus, the average flow deviates from that computed directly in terms of the measured flow rate in LPM. Instead the flow velocity is obtained by multiplying the computed value of U_{in} by a scaling factor β that is empirically defined as $\beta = |U_{in}/U_{in}^*|^{0.9}$, where $U_{in}^* \triangleq 1$ m/s, making β a dimensionless quantity. A zero-mean Gaussian noise of standard deviation $0.3 Pa$ has been added to the output in order to emulate the process noise as well as the sensor noise. This choice is made to match the (non-dimensional) P_{rms} value described in Section 4.3. The numerical sensor measures the acoustic pressure of each Galerkin-mode and then computes the combined acoustic pressure at that location following Equation (2).

For the remainder of the paper, the parameter values described in this section have been used without any changes. In other words, with these parameters optimised a complete model of the system is obtained, and the only changes that need to be made for each numerical experiment are the boundary conditions.
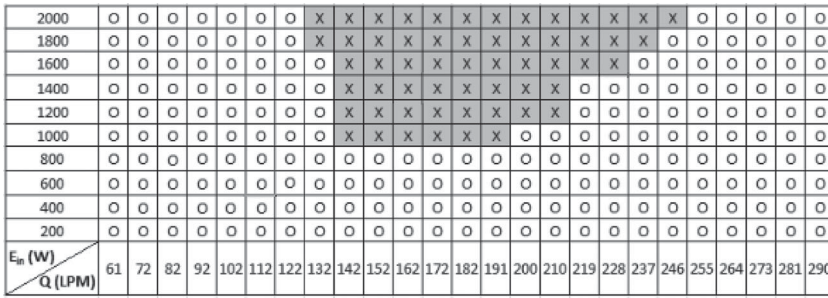
E_{in} (W) / Q (LPM)	61	72	82	92	102	112	122	132	142	152	162	172	182	191	200	210	219	228	237	246	255	264	273	281	290
2000	o	o	o	o	o	o	o	x	x	x	x	x	x	x	x	x	x	x	x	x	o	o	o	o	o
1800	o	o	o	o	o	o	o	x	x	x	x	x	x	x	x	x	x	x	x	o	o	o	o	o	o
1600	o	o	o	o	o	o	o	o	x	x	x	x	x	x	x	x	x	x	o	o	o	o	o	o	o
1400	o	o	o	o	o	o	o	o	x	x	x	x	x	x	x	x	o	o	o	o	o	o	o	o	o
1200	o	o	o	o	o	o	o	o	x	x	x	x	x	x	x	x	o	o	o	o	o	o	o	o	o
1000	o	o	o	o	o	o	o	o	x	x	x	x	x	x	o	o	o	o	o	o	o	o	o	o	o
800	o	o	o	o	o	o	o	o	o	o	o	o	o	o	o	o	o	o	o	o	o	o	o	o	o
600	o	o	o	o	o	o	o	o	o	o	o	o	o	o	o	o	o	o	o	o	o	o	o	o	o
400	o	o	o	o	o	o	o	o	o	o	o	o	o	o	o	o	o	o	o	o	o	o	o	o	o
200	o	o	o	o	o	o	o	o	o	o	o	o	o	o	o	o	o	o	o	o	o	o	o	o	o

Figure 2. Stability map generated from experimental data of Rijke tube apparatus. Instability indicated by dark shading marked with ' × ', and stability by light shading with '°'.

4. Stability maps developed from experimental data and model data

This section develops and compares stability maps from data generated from the Rijke tube apparatus (see Section 2) and reduced-order model (see Section 3.4) under the same operating conditions.

4.1. *Stability map: experimental data*

Experiments have been conducted with multiple combinations of heater power input (E_{in}) and air flow rate (Q) to record data of 30 s duration for each case. A typical stability map is shown in Figure 2 with the following notations: the spaces marked as ' × ' (with a darker shaded box) denote unstable operation with an audibly discernible resonating mode, and those marked as '°' (with lighter shading) denote stable operation.

Different values of initial temperatures affect the stability characteristics of the thermoacoustic process as a consequence of changes in the mean temperature in the Rijke tube. When a lower initial mean temperature of around $\sim 300°$K is maintained in the Rijke tube apparatus, a lower frequency (~ 114 Hz) mode of instability is observed; the instability occurred at a higher frequency (~ 131 Hz) mode at a higher initial mean temperature of $\sim 348°$K. These observations are attributed to the increase in the speed of sound at an elevated mean temperature, which changes the fundamental frequency from an analytically calculated value of 115– 127 Hz for an open-open tube, tallying closely with the peak frequencies of experimental data. In this work, only the higher initial temperature mode has been reported for validation because it is more consistent and is easier to obtain experimentally because cooling the Rijke tube after each experiment is very time-consuming.

4.2. *Stability map: numerical simulation of the reduced-order model*

The reduced-order model, described in Section 3, has been run with the same model parameters for the same range of flow rates and primary heater power inputs as the experiments described above. The ambient temperature is taken to be 348°K, which is the more appreciable ambient conditions as described above. Each simulation has been performed for simulated time intervals of 30 s with a time step size $\Delta t = 10^{-4}$ s; and the root mean square (RMS) values of pressure oscillations are computed over the last 2 s as a measure of stability. An operational condition is considered to be unstable if the P_{rms} exceeds a threshold

Primary Power (in W)	61	72	82	92	102	112	122	132	142	152	162	172	182	191	200	210	219	228	237	246	255	264	273	281	290
2000	0	0	0	0	0	0	0	1	1	1	1	1	1	1	1	1	1	1	1	1	1	0	0	0	0
1800	0	0	0	0	0	0	0	1	1	1	1	1	1	1	1	1	1	1	1	1	0	0	0	0	0
1600	0	0	0	0	0	0	0	0	1	1	1	1	1	1	1	1	1	1	0	0	0	0	0	0	0
1400	0	0	0	0	0	0	0	0	1	1	1	1	1	1	1	1	1	1	0	0	0	0	0	0	0
1200	0	0	0	0	0	0	0	0	1	1	1	1	1	1	1	1	1	0	0	0	0	0	0	0	0
1000	0	0	0	0	0	0	0	0	0	1	1	1	1	1	1	0	0	0	0	0	0	0	0	0	0
800	0	0	0	0	0	0	0	0	0	0	0	0	0	0	0	0	0	0	0	0	0	0	0	0	0
600	0	0	0	0	0	0	0	0	0	0	0	0	0	0	0	0	0	0	0	0	0	0	0	0	0
400	0	0	0	0	0	0	0	0	0	0	0	0	0	0	0	0	0	0	0	0	0	0	0	0	0
200	0	0	0	0	0	0	0	0	0	0	0	0	0	0	0	0	0	0	0	0	0	0	0	0	0

Flowrate (in LPM)

Figure 3. Stability map generated from simulation data of reduced-order model. Instability indicated by dark shading marked with '1', and stability by light shading with '0'.

of 5 Pa. The generated stability map is shown in Figure 3. The boxes shaded darker blue with the Boolean value of 1 indicates an unstable operating condition.

It is seen that the stability map matches very closely with that reported from experiments (shown in Figure 2). A comparison of the stability in Figures 2 and 3 reveals that, in the physical experiments, the maximum range of unstable operation is bounded in the power range 1000– 2000 W and in flow range 132–246 LMP. For the numerical simulation, the power range 1000–2000 W is identical to that in experiments, while the flow rate range is 132–255 LPM, which is reasonably close. The frequency of the unstable mode was also found to be 117 Hz which is very close to the experimentally obtained value of 131 Hz.

A comparison of the experimental stability map and numerical stability map reveals that the discrepancies occur for 7 out of 57 unstable conditions, yielding an error rate of about 12%. This discrepancy is possibly due to the fact that the numerical model is a deterministic model of a stochastic process with a few outliers. In addition, there may be certain experimental uncertainties such as the exact ambient temperature, the exact initial condition of the tube, both of which are not perfectly repeatable. There are also some modelling simplifications that may tend to lead to inaccuracies towards the edges of the unstable region seen in the stability map. However, for the purpose at hand, a higher-fidelity model may not be necessary because this low-fidelity model yields a sufficiently close match to the experimental ground truth. For another Rijke tube, the parameters (e.g. damping coefficients c_1 and c_2) of the numerical model should be tuned to match the experimental data.

It is also worthwhile to note that although theproposed reduced-order model is more detailed than the traditional Galerkin-based models (which do not account for heater effects or thermal inertia), the time required to run a simulation is reasonably low. In practice, it is observed that the simulation time required is approximately $1.5\times$ (i.e. simulation of a time interval of 30 s takes $\sim$ 45 s of the machine run-time). The code has been developed and run on MATLAB 2019b utilising a single core of an Intel Xeon Workstation using the E5-2670 chipset.

4.3. *Comparison of numerical simulation and experimental results*

A major focus of this paper is to incorporate the thermal inertia of the heaters in the model equations and to investigate the effects of the same on the system dynamics of the Rijke tube. In order to study these phenomena, each experiment has been conducted
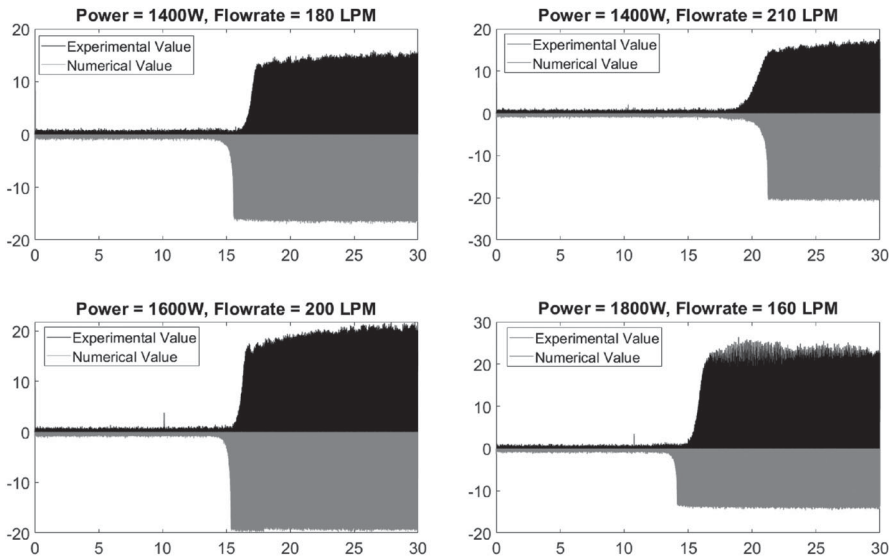
Figure 4. Time series of pressure oscillations: experimental and simulation data, where the upper parts (in black) are experimentally observed time series and the lower parts (in grey) are numerically simulated from the reduced-order model under the same operating conditions.

for a duration of 30 s in the following fashion. The heater power is maintained at 200 W for the first 10 s and then the heater power is abruptly increased to the final value. It is noted that the resulting increase in the heater temperature is not linear over the entire period. Furthermore, there is a process-dependent time delay between the heater power and heater temperature responses. As mentioned before, many reduced-order numerical models do not capture this behaviour. The model proposed in this paper incorporates the heater dynamics, and thus captures these delays in the formulation of the reduced-order model.

The four plates in Figure 4 display four profiles of pressure oscillations to compare the dynamic behaviour of the Rijke tube both in the experiment as well as in the numerical simulation under four different operating conditions. The primary power is maintained at 1400, 1600 and 1800 W as shown in the figure. For all of these runs, the secondary heater is kept inactive. For each of the operating condition reported here, the upper part (in black) of Figure 4 shows the pressure profile obtained from experiments following the same power profile. The lower part (in grey) of Figure 4 shows the equivalent numerical simulation. These responses have been scaled for ease of comparison, where the scaling factor has been chosen to be the root mean square (RMS) value of the noise. With this scale factor, the peak values of the numerically obtained instabilities match those that are obtained experimentally; from these observations, the noise in the reduced-order model is identified to be a zero-mean Gaussian with intensity 0.3 Pa.

Form the results of comparisons in Figure 4, it is concluded that the model-predicted instability growth is very close to that observed in the experimental results. This observation suggests that the numerical model is capable of capturing the Rijke tube dynamics very well, which include heater dynamics and delays. The small deviations between the model predictions and experimental observations, as seen in Figures 2 and 3 and in the four plates of Figure 4, can be attributed to the uncertainties in modelling of experimental conditions.
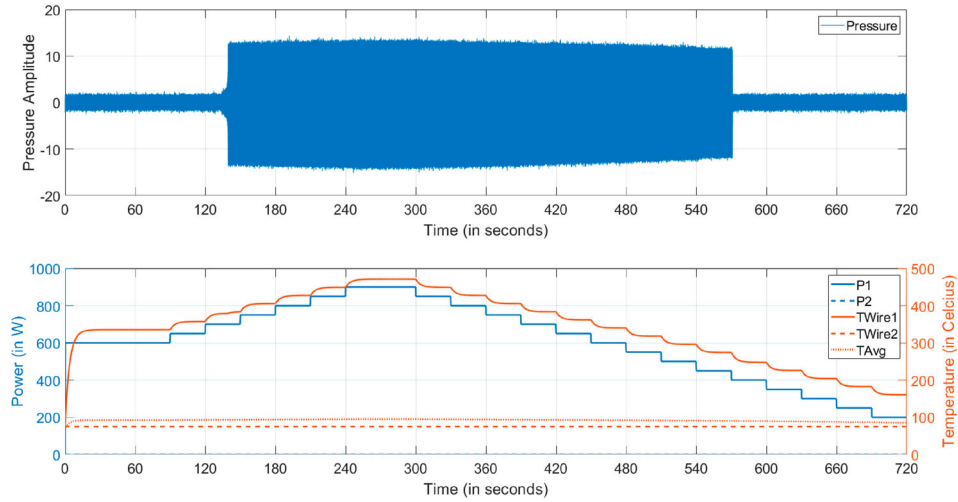
Figure 5.   Time series of hysteresis experiment simulation.

4.4.   *Hysteresis as a result of thermal dynamics*

It has been observed by [4] that the onset of instability in the Rijke tube exhibits hysteresis due to the thermal inertia of the system. The rationale is that the direction of approaching a particular operating condition may change depending on whether that it is stable or unstable; this effect is seen in the simulation as well. In order to observe the hysteresis phenomena, the simulation has been conducted for a total of 720 s duration when the air flow rate is held constant at 160 LPM and the primary heater power is varied in the following way. For the first 90 s, the primary heater power is held at 600 W to ensure that a steady state is reached. Subsequently, the primary heater power is increased in steps of 50 W on an interval of 30 s. Holding the power constant for each window of 30 s ensures that a quasi-steady state is reached for the respective power setting. These stepwise increments are continued till the power reaches a maximum of 900 W. The system is held steady at a power of 900 W for a minute and then the process is reversed by reducing the power in decrements of 50 W every 30 s. It is seen that the system remains unstable even at 600 W during the decreasing power steps although the system was initially stable at 600 W as seen in Figure 3. Therefore, the decrements in power are continued till a lower bound of 200 W is reached as seen in Figure 5.

The top part in Figure 5 shows the profile of pressure signal for the above numerical experiment, while the bottom part shows the temporal variations in power and the average (wire) temperature of the two heaters in the Rijke tube apparatus: *P1* and *TWire1* for the primary heater, and *P2* and *TWire2* for the secondary (inactive) heater. It is seen that the temperature profile has a lag as compared to the heater power profile, which is an effect of the thermal dynamics; these phenomena have not been captured by most reduced-order numerical models. Figure 6 presents the hysteresis loop for the numerical experiment, where the changes in the RMS values (P_{rms}) of the pressure oscillations over the last 5 s of each 30 s window are shown along with the arrows that indicate the direction of the primary heater power being varied.
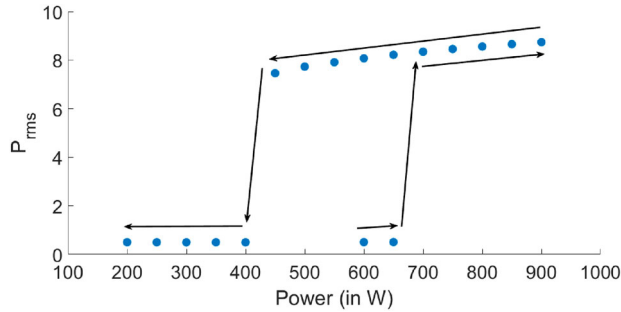
Figure 6. Hysteresis loop obtained from the simulation in Figure 5.

Following Figure 6, the system becomes unstable at $\sim 700\,\text{W}$ while the power is increased (i.e. forward path in the hysteresis diagram). However, as per the stability chart in Figure 3, this operational condition is expected to be stable. Further increasing the power to 900 W only increases the amplitude of the pressure oscillations, but the system still remains unstable. On the return path, however, the system stays unstable past 700 W and remains unstable right down till $\sim 450\,\text{W}$. At $\sim 400\,\text{W}$, the system finally returns to stability and remains stable for lower values of power. As seen in Figure 6, this leads to a reasonably large hysteresis loop, very similar to what was reported by [4].

5. Simulated control using the secondary heater

This section presents a numerical simulation of active control of the Rijke tube system by manipulating the power of the secondary heater while that of the primary heater is held constant. Having the dynamical model of the Rijke tube validated with experimental data, numerical simulations have been performed to test the efficacy of the secondary heater as a (passive) controller to suppress the thermoacoustic oscillations.

Usage of a secondary heat source for active control of thermoacoustic instabilities has been addressed in the technical literature (e.g. [20,26]. To this end, the researchers have placed a secondary electric heater downstream in the flow path of the Rijke tube to control the instabilities, where a Bunsen burner served as the primary heat source; this concept has been validated both numerically and experimentally. However, the numerical simulations have not included the heater dynamics and therefore yielded nearly instantaneous control, which is different from real-life experiments. The current paper has included the effects of heater dynamics and compared the results with the findings of [20]. In the current paper, all controllers are passive with no feedback loop because the primary aim is to show the effectiveness of the secondary heater for control of thermoacoustic pressure oscillations and the expected time delays due to the system dynamics.

5.1. *Simulated control: effectiveness of control heater*

In order to demonstrate its efficacy as a controller, the secondary heater has been placed at $x_2 = 1.125\,\text{m}$, which is about three-quarters of the length down the Rijke tube. This location has been demonstrated by [4] to be most effective for suppressing thermoacoustic instabilities in the Rijke tube when the primary heater is placed at a quarter length down
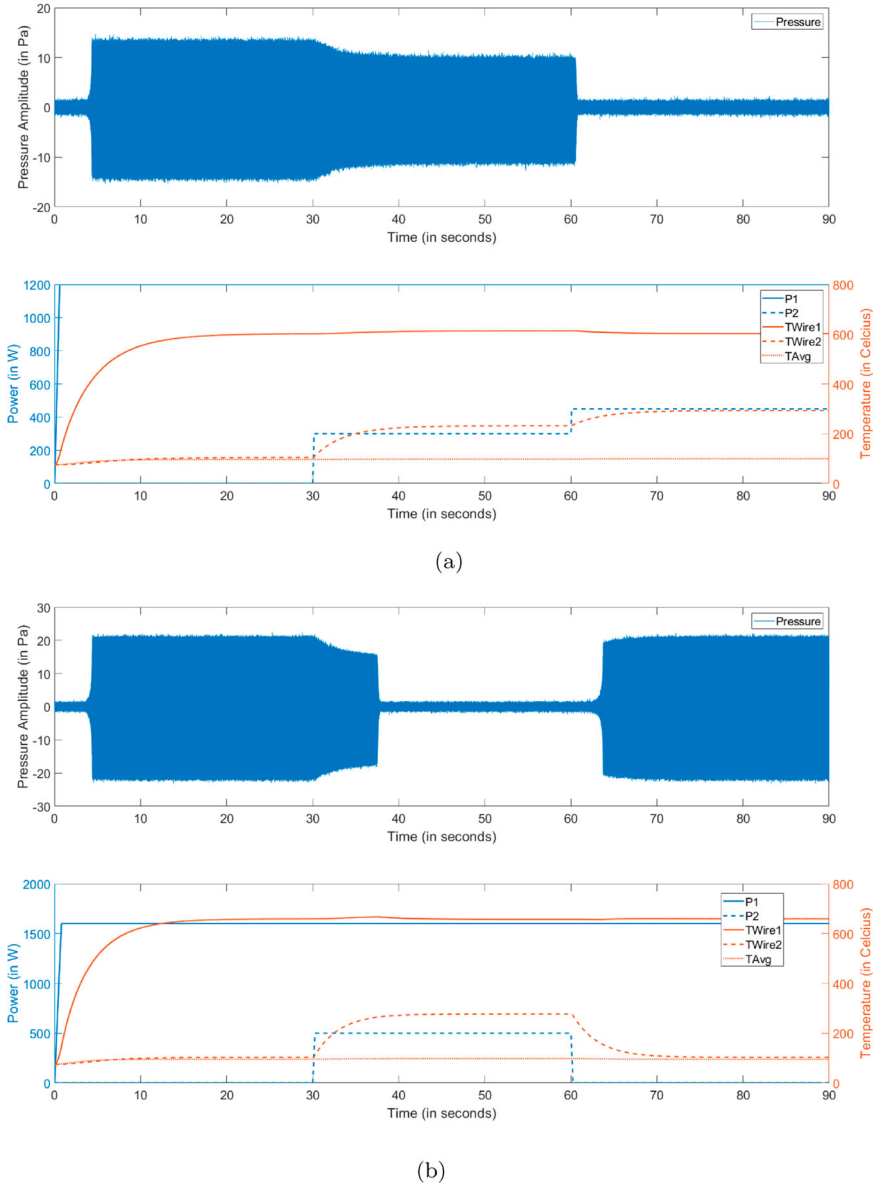
(a)

(b)

Figure 7. Time series of pressure, temperature, and power in two simulated control experiments. (a) Time series from the first control case: flow rate of 140 LPM and (b) time series from the second control case: Flow rate of 210 LPM.

from the inlet. Two trial cases are conducted to demonstrate the effects of the secondary heater and the results are shown in Figure 7.

The first case consists of numerical simulations for a time interval of 90 s with a constant flow rate of 140 LPM. At the very start (i.e. time $t = 0$ s), as the primary heater power is increased to 1200 W, the system becomes unstable. The primary power is then held at a constant level of 1200 W for 90 s, while leaving the secondary heater turned

off. At time $t = 30$ s, the secondary heater power is increased to 300 W and then further increased to 450 W at $t = 60$ s. The profiles of the corresponding pressure time series and associated power and temperature time series are shown in Figure 7(a). It is seen that although the secondary heater power at 300 W is incapable of completely suppressing the thermoacoustic instabilities, it modestly reduces the amplitude of the pressure oscillations. However, increasing the secondary power to 450W completely suppresses the high-amplitude pressure oscillations.

The second case consists of numerical simulations for a time interval of 90 s with a constant flow rate of 210 LPM. At time $t = 0$ s, the primary heater power is increased to 1600 W while the secondary heater is kept off till $t = 30$ s and then raised to 500 W; the secondary heater is switched off at $t = 60$ s. The corresponding pressure time series and the associated power and temperature time series are shown in Figure 7(b). It is seen that the initially unstable system is adequately controlled by switching on the secondary heater. However, when the secondary heater is switched off, the system reverts back to instability.

5.2. *Simulated control: effect of control heater location*

The location of the control (secondary) heater largely determines whether the instability would be successfully suppressed. To demonstrate this phenomenon, numerically, two cases have been considered, each having a simulated time interval of 460 s. In both cases, the air flow rate is kept constant at 180 LPM and, at $t = 0$ s, the primary heater power is raised to 1400 W; at $t = 20$ s, the secondary heater power is increased to 600 W. As seen in Figure 8(a), the instability is completely suppressed. Figure 8(b) shows that, although the amplitude is very modestly reduced, the pressure oscillations still prevail. This is due to the fact that the secondary heater is located at $x_2 = 1.125$ m (i.e. 3L/4 from inlet) for first case (Figure 8(a)), which is the most effective location for control. In contrast, for Figure 8(b), the secondary heater is placed further upstream at $x_2 = 0.875$ m (i.e. 7L/12 from inlet).

5.3. *Simulated control: comparison with results reported in technical literature*

In their research, [20] studied the effects of location of the secondary heater on suppression of thermoacoustic instabilities in a Rijke tube. It was observed that, for a particular operating condition, placing the secondary heater at 0.73 L causes the minimum power needed to mitigate instability to be 122.5 W in their apparatus. Placement of the secondary heater at 0.80 and 0.87 L causes the needed minimum power levels to be 183 and 309 W, respectively.

In the current paper, similar numerical simulations have been conducted for the flow rate of 210 LPM and primary power of 1200 W. When the secondary heater is placed at 0.73 L(1.095 m), the minimum power needed to completely suppress the oscillations is found to be $\sim$ 268 W; and when the heater is placed at 0.80 L(1.2 m)and 0.87 L(1.305 m), the minimum power requirements are $\sim$ 326 and $\sim$ 513 W, respectively. Thus, a very similar trend is observed between the numerical simulations presented in this paper and those generated experimentally by [20]. The values do not match exactly because of the following reasons. The Rijke tube geometries are different and the primary heat source in the experimental work by [20] is a flame while the heat source in the numerical model, presented in this paper, is an electric heater; hence the input conditions are dissimilar.
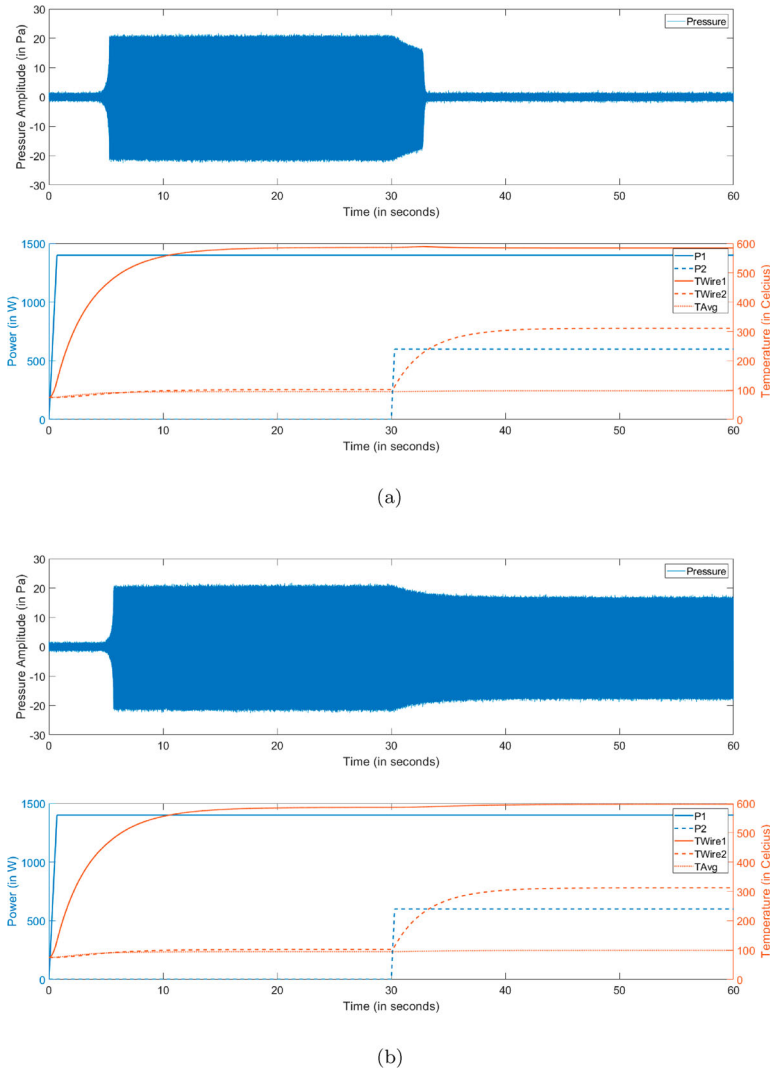
(a)

(b)

Figure 8. Effects of the control heater location on system dynamics. (a) Time series of pressure, temperature, and power in the simulation with the control heater placed at $x_2 = 1.125$ m (3L/4) and (b) time series of pressure, temperature, and power in the simulation with the control heater placed at $x_2 = 0.875$ m (7L/12).

6. Summary, conclusions, and future work

This paper has proposed a modification of the traditional Galerkin-mode-based technique to construct a reduced-order model of an (electrically heated) Rijke tube, which includes the inherent thermal physics of the heaters and the system dynamics in general. The model equations are developed by including the heat transfer phenomena in the heaters and thermoacoustics in the Rijke tube. This approach yields realistic time lags which are critical for evaluating dynamic performance and system stability for real-time monitoring and active control. The model structure is flexible in the sense that it is capable of incorporating either

a single heater or a combination of two heaters, where typically the secondary heater acts as an actuator for controlling the thermoacoustic instabilities.

The single-heater reduced-order model has been validated with experimental data collected from the Rijke tube apparatus, and the numerical results of the reduced-order model have yielded very good agreement with those obtained experimentally. The performance of the two-heater model has been tested by numerical simulation and is seen to function as expected. Numerical results of the two-heater model are compared with those of other available models, reported in open literature, which are also in good agreement. The numerical simulations show the effectiveness of the secondary heater as a (passive) controller.

The following topics are suggested for future research:

(1) Experimental validation of the two-heater model results on the Rijke tube apparatus.
(2) Detailed analysis of the fundamental frequencies in the system dynamics to serve as indicators of anomalous operations.
(3) Analysis and synthesis of a robust controller for real-time active control of thermoacoustic instabilities based on the two-heater numerical model.
(4) Implementation and testing of the above active controller on the Rijke tube apparatus.

Disclosure statement

No potential conflict of interest was reported by the authors.

Funding

References

[1] J.W.S. Rayleigh, *The Theory of Sound*, Dover, New York, 1845.
[2] S. Candel, *Combustion dynamics and control: Progress and challenges*, Proc. Combust. Inst. 2(9) (2002), pp. 1–28.
[3] P.L. Rijke, *Notiz über eine neue art, die in einer an beiden enden offenen řhre enthaltene luft in schwingungen zu versetzen*, Ann. Phys. 18(3) (1859), pp. 339–343.
[4] K.I. Matveev, *Thermoacoustic instabilities in the rijke tube: Experiments and modeling*, Ph.D. diss., California Institute of Technology, 2003.
[5] L. Kabiraj and R.I. Sujith, *Nonlinear self-excited thermoacoustic oscillations: Intermittency and flame blowout*, J. Fluid. Mech. 71(3) (2012), pp. 376–397.
[6] D. Zhao, *Transient growth of flow disturbances in triggering a Rijke tube combustion instability*, Combust. Flame. 15(9) (2012), pp. 2126–2137.
[7] D. Zhao and Z.H. Chow, *Thermoacoustic instability of a laminar premixed flame in Rijke tube with a hydrodynamic region*, J. Sound. Vib. 33(2) (2013), pp. 3419–3437.
[8] A. Sjunnesson, P. Henrikson, and C. Lofstrom, *CARS measurements and visualization of reacting flows in a bluff body stabilized flame*, in *28th Joint Propulsion Conference and Exhibit, Joint Propulsion Conferences*, 1992.
[9] A. Fichera, C. Losenno, and A. Pagano, *Experimental analysis of thermo-acoustic combustion instability*, Appl. Energy. 7 (2001), pp. 179–191.

[10] J.G. Lee and D.A. Santavicca, *Experimental diagnostics for the study of combustion instabilities in lean premixed combustors*, J. Propul. Power 1(9) (2003), pp. 735–750.

[11] F. Richecoeur, S. Ducruix, P. Scouflaire and S. Candel, *Experimental investigation of high-frequency combustion instabilities in liquid rocket engine*, Acta. Astronaut. 6(2) (2008), pp. 18–27.

[12] U. Sen, T. Gangopadhyay, C. Bhattacharya, A. Misra, P.S.S. Karmakar, A. Mukhopadhyay, and S. Sen, *Investigation of ducted inverse nonpremixed flame using dynamic systems approach*, in *ASME Turbo Expo 2016: Turbomachinery Technical Conference and Exposition*, Vol. 4B, 2016.

[13] F.E.C. Culick, *Nonlinear behavior of acoustic waves in combustion chambers-I*, Acta. Astronaut. 3 (1976), pp. 715–734.

[14] M.A. Heckl, *Active control of the noise from a Rijke tube*, J. Sound. Vib. 12(4) (1988), pp. 117–133.

[15] M.A. Heckl, *Non-linear acoustic effects in the Rijke tube*, Acustica 7(2) (1990), pp. 63–71.

[16] P. Subramanian, S. Mariappan, R.I. Sujith, and P. Wahi, *Bifurcation analysis of thermoacoustic instability in a horizontal rijke tube*, Int. J. Spray Combust. Dyn. 2 (2010), pp. 325–355.

[17] G.A. Richards, D.L. Straub, and E.H. Robey, *Passive control of combustion dynamics in stationary gas turbines*, J. Propul. Power 1(9) (2003), pp. 795–810.

[18] D. Zhao and A. Morgans, *Tuned passive control of combustion instabilities using multiple Helmholtz resonators*, J. Sound. Vib. 32 (2009), pp. 744–757.

[19] N.N. Deshmukh and S. Sharma, *Experiments on heat content inside a Rijke tube with suppression of thermo-acoustics instability*, Int. J. Spray Combust. Dyn. 9 (2017), pp. 85–101.

[20] D. Zhao, C. Ji, X. Li, and S. Li, *Mitigation of premixed flame-sustained thermoacoustic oscillations using an electrical heater*, Int. J. Heat. Mass. Transf. 8(6) (2015), pp. 309–318.

[21] S. Mondal, N.F. Ghalyan, A. Ray, and A. Mukhopadhyay, *Early detection of thermoacoustic instabilities using hidden Markov models*, Combust. Sci. Technol. 19(1) (2019), pp. 1309–1336.

[22] F.E.C. Culick, *Combustion instabilities in liquid-fuelled propulsion systems*, AGARD-CP-450, 1988.

[23] K.I. Matveev and F.E.C. Culick, *A model for combustion instability involving vortex shedding*, Combust. Sci. Technol. 17(5) (2003), pp. 1059–1083.

[24] V. Nair, R.I. Sujith, *A reduced-order model for the onset of combustion instability: Physical mechanisms for intermittency and precursors*, in *Proceedings of the Combustion Institute*, Vol. 35, 2015, pp. 3193–3200

[25] J.R. Andrews, *Temperature Dependence of Gas Properties in Polynomial Form*, The NPS Institutional Archive DSpace Repository, Calhoun, 1981.

[26] X. Jin, H. Zhao and S. Li, *Experimental and numerical study of passive control of self-sustained thermoacoustic oscillations using an electrical heater*, Energy Procedia 105 (2017), pp. 4661–4667. 8th International Conference on Applied Energy, ICAE2016, 8–11 October 2016, Beijing, China.